

## Supporting Information Appendix

### **A repeat protein links Rubisco to form the eukaryotic carbon-concentrating organelle**

Luke C. M. Mackinder<sup>a</sup>, Moritz T. Meyer<sup>b</sup>, Tabea Mettler-Altmann<sup>c,1</sup>, Vivian K. Chen<sup>a,d</sup>, Madeline C. Mitchell<sup>b,2</sup>, Oliver Caspari<sup>b</sup>, Elizabeth S. Freeman Rosenzweig<sup>a,d</sup>, Leif Pallesen<sup>a</sup>, Gregory Reeves<sup>a,3</sup>, Alan Itakura<sup>a,d</sup>, Robyn Roth<sup>e</sup>, Frederik Sommer<sup>c,4</sup>, Stefan Geimer<sup>f</sup>, Timo Mühlhaus<sup>c,4</sup>, Michael Schroda<sup>c,4</sup>, Ursula Goodenough<sup>e</sup>, Mark Stitt<sup>c</sup>, Howard Griffiths<sup>b</sup>, Martin C. Jonikas<sup>a,d,5</sup>

<sup>a</sup>Carnegie Institution for Science, Department of Plant Biology, Stanford, California 94305, USA.

<sup>b</sup>Department of Plant Sciences, University of Cambridge, Cambridge CB2 3EA, UK. <sup>c</sup>Max Planck Institute of Molecular Plant Physiology, 14476 Potsdam-Golm, Germany. <sup>d</sup>Department of Biology, Stanford University, Stanford, CA 94305, USA. <sup>e</sup>Department of Biology, Washington University, St. Louis, Missouri 63130, USA. <sup>f</sup>Cell Biology & Electron Microscopy, University of Bayreuth, 95440 Bayreuth, Germany.

Present addresses: <sup>1</sup>Cluster of Excellence in Plant Sciences and Institute of Plant Biochemistry, Heinrich-Heine-University, 40225 Düsseldorf, Germany; <sup>2</sup>Agriculture, Commonwealth Scientific and Industrial Research Organisation, Canberra, ACT 2601, Australia; <sup>3</sup>Department of Plant Sciences, University of Cambridge, Cambridge CB2 3EA, UK; <sup>4</sup>Institute of Molecular Biotechnology and Systems Biology, Technical University of Kaiserslautern, 67663 Kaiserslautern, Germany.

<sup>5</sup>To whom correspondence should be addressed. Email: [mjonikas@carnegiescience.edu](mailto:mjonikas@carnegiescience.edu). Telephone: +1 650 739 4216

## SI Materials and Methods

### Strains and culture conditions

*Chlamydomonas reinhardtii* strain CC-1690 was maintained at 22°C with 55  $\mu\text{mol photons m}^{-2} \text{s}^{-1}$  light on tris-acetate-phosphate (TAP) (56) agar (1.4%) plates containing 0.4% Bacto-Yeast extract (Becton, USA). The cMJ030 wild-type (WT) and *epyc1* mutant were maintained in the dark or low light ( $\sim 10 \mu\text{mol photons m}^{-2} \text{s}^{-1}$ ) on 1.5% agar plates containing TAP with revised (57) or traditional Hutner's trace elements (58).

For proteomics analysis, a 50 mL pre-culture was grown mixotrophically in TAP on a rotatory shaker at 124 rpm, 22°C and under an illumination of 55  $\mu\text{mol photons m}^{-2} \text{s}^{-1}$  for three days according to Mettler *et al.* (59). In brief, a second pre-culture of 500 mL was used to inoculate a 5-litre bioreactor BIOSTAT®B-DCU (Sartorius Stedim, Germany). The absence of contamination was monitored according to Mettler *et al.* (59). Cultures with a cell density of  $3\text{-}5 \times 10^6 \text{ cells mL}^{-1}$  were grown photoautotrophically at 46  $\mu\text{mol photons m}^{-2} \text{s}^{-1}$  light in air enriched with high CO<sub>2</sub> (5% CO<sub>2</sub>) under constant turbidity for two days before the culture was aerated with low CO<sub>2</sub> (ambient air; 0.039% CO<sub>2</sub>). The CO<sub>2</sub> level in the outlet air of the bioreactor was measured by an on-line multi-valve gas chromatograph (3000A MicroGC run by EZChromElute software, Agilent Technologies, USA). After switching from high to low CO<sub>2</sub>, the CO<sub>2</sub> dropped from 4.5% to a constant 0.02% after 12 hours. Cells were harvested at 30 hours after the shift to low CO<sub>2</sub>.

For mRNA levels, O<sub>2</sub> evolution, Rubisco content western blotting, pyrenoid size analysis by transmission electron microscopy (TEM) and Rubisco subcellular localization by immuno-gold labelling, strains were grown photoautotrophically in 50 mL tris-minimal medium (58) under constant aeration, shaking and illumination (150 rpm, 21°C, 50-65  $\mu\text{mol photons m}^{-2} \text{s}^{-1}$ ; Infors HT Multitron Pro, Switzerland). Briefly, starter cultures were inoculated from freshly re-plated cultures on TAP plates, to 0.3  $\mu\text{g chlorophyll (a+b) mL}^{-1}$ , and aerated with high CO<sub>2</sub> (5% v/v CO<sub>2</sub> enriched air). When cell density reached mid-log ( $\sim 3 \mu\text{g chlorophyll (a+b) mL}^{-1}$ ), half of the cultures were harvested and analysed. The remaining half of the cultures were then switched to aeration with low CO<sub>2</sub> (air, 0.04% v/v CO<sub>2</sub>) for induction of the CCM. For gene expression analysis and affinity for inorganic carbon, cells were air-adapted for 3 hours, corresponding to peak induction of CO<sub>2</sub>-inducible genes (60-62). The state of CCM induction was controlled by measuring the mRNA accumulation of a highly CO<sub>2</sub>-responsive gene, *LCII* (Cre03.g162800). For TEM analysis of pyrenoid size and immuno-gold labelling of Rubisco, cells were adapted to low CO<sub>2</sub> for 24 hours.

For EPYC1 protein abundance and freeze fracture cryo-electron microscopy of WT and mutant cells, cultures were propagated continuously in tris-phosphate (TP) (57) medium with 50  $\mu\text{mol photons m}^{-2} \text{s}^{-1}$  light for  $\sim 1$  week in a Multi-Cultivator (Photon Systems Instruments) with bubbling of high CO<sub>2</sub> (3% v/v CO<sub>2</sub>). Cells were diluted every 24 hours to ensure they were kept in the log phase. 6 hours before sampling, half of the cultures were switched from high CO<sub>2</sub> to low CO<sub>2</sub> (air,  $\sim 0.04\%$  v/v CO<sub>2</sub>). The chlorophyll concentration at harvesting was  $\sim 3 \mu\text{g chlorophyll (a+b) mL}^{-1}$ .

For fluorescence microscopy and RbcS1-mCherry localization experiments, cells were grown in TP medium containing antibiotics used for selection of expression of the fluorescently labeled gene (Venus, paromomycin at  $2 \mu\text{g mL}^{-1}$ ; mCherry, hygromycin  $6.25 \mu\text{g mL}^{-1}$ ), bubbled with high  $\text{CO}_2$  (3% v/v  $\text{CO}_2$ ) at a  $150 \mu\text{mol photons m}^{-2} \text{s}^{-1}$  light intensity. At  $\sim 2 \times 10^6 \text{ cells mL}^{-1}$ , after >6 doublings, cells were transferred to low  $\text{CO}_2$  for 14 hours. For the RbcS1-mCherry localization experiments, samples were taken and imaged immediately before the switch to low  $\text{CO}_2$  and after 14 hours at low  $\text{CO}_2$ .

For co-immunoprecipitation experiments, cells were grown in 50 mL of TAP at  $150 \mu\text{mol photons m}^{-2} \text{s}^{-1}$  light until  $\sim 2\text{-}4 \times 10^6 \text{ cells mL}^{-1}$ , centrifuged at 1000 g for 4 min, resuspended in TP and used to inoculate 800 mL of TP. Cells were then bubbled with low  $\text{CO}_2$  (air,  $\sim 0.04\%$  v/v  $\text{CO}_2$ ) at  $150 \mu\text{mol photons m}^{-2} \text{s}^{-1}$  until  $\sim 2\text{-}4 \times 10^6 \text{ cells mL}^{-1}$  and harvested as indicated below. All liquid media contained  $2 \mu\text{g mL}^{-1}$  paromomycin.

Cell concentrations were measured using a Z2 Coulter Counter (Beckman Coulter, USA).

## **Proteomics of pyrenoid-enriched fraction**

### *Pyrenoid enrichment*

10 mL algal material ( $3\text{-}5 \times 10^6 \text{ cells mL}^{-1}$ ) were harvested by centrifugation for 2 min ( $3,220 \times g$ ,  $4^\circ\text{C}$ ), immediately frozen in liquid nitrogen and extracted with extraction buffer (EB; 50 mM HEPES,  $20 \mu\text{M}$  leupeptin, 1 mM PMSF, 17.4% glycerol, 2% Triton). The samples were sonicated 6 x 15 s (6 cycles, 50% intensity, Sonoplus Bandelin Electronics, Germany) and kept on ice between cycles for 90 s. The samples were centrifuged at 500 g for 3 min to obtain a soluble and pellet fraction. This procedure resembled the first steps of a protocol used in previous studies (38, 39). The pellet was washed three times with 1 mL, 500  $\mu\text{L}$  and 300  $\mu\text{L}$  EB before resuspension in 100  $\mu\text{L}$  50 mM ammonium bicarbonate. Protein concentrations were measured by Lowry assay using BSA as a standard (63).

### *SDS-PAGE*

For SDS-PAGE, samples were resuspended in a buffer containing 50 mM dithiothreitol (DTT), 50 mM sodium-carbonate, 15% sucrose (w/v) and 2.5% SDS (w/v), heated 45 seconds at  $95^\circ\text{C}$  and spun down at  $16,700 \times g$  before applying 22  $\mu\text{g}$  total protein to the polyacrylamide gel. The 14%-separating gel was stained with Coomassie Brilliant Blue (64).

### *Protein digestion and mass spectrometric analysis*

For shotgun proteomics, samples were prepared and measured according to Mhlhaus *et al.* (40). In brief, 20  $\mu\text{g}$  protein per sample was precipitated in 80% acetone at  $-20^\circ\text{C}$  over night. The precipitated proteins were resuspended in 6 M urea and 2 M thiourea (in 50 mM ammonium hydrogen carbonate), reduced by DTT, carbamidomethylated with iodoacetamide, digested with endoproteinase LysC (Roche, Switzerland) and immobilised trypsin (Applied Biosystems, Thermo Fisher Scientific, USA), and subsequently desalted according to Mhlhaus *et al.* (40). The resuspended peptides were acidified with 1% acetic acid. Peptides were chromatographically separated by reverse

phase separation with a nanoUPLC (nanoACQUITY UPLC, Waters, Milford, USA) using a 10 cm x 75  $\mu\text{m}$  BEH130 C18 1.7  $\mu\text{m}$  particles (Waters) column for separation and a 2 cm x 180  $\mu\text{m}$  Symmetry C18 5  $\mu\text{m}$  particles (Waters) column for trapping. Peptides were analysed by a linear trap quadrupole-Orbitrap mass spectrometer (Thermo Fisher Scientific, USA) according to Mühlhaus *et al.* (40).

#### *Data processing and data analysis*

Raw MS files were processed with MaxQuant (version 1.5.2.8) (41). Peak list files were searched against *Chlamydomonas reinhardtii* gene model JGIv4 from Phytozome 10.2 (<http://phytozome.jgi.doe.gov/>) including the organelle genome sequences. Maximum precursor and fragment mass deviations were set to 20 ppm and 0.5 Da. Peptides with at least six amino acids were considered for identification. The search included carbamidomethylation as a fixed modification and variable modifications for oxidation of methionine and protein N-terminal acetylation. The false discovery rate, determined by searching a reverse database, was set at 0.01 for both peptides and proteins. Identification across different replicates and treatments was achieved by enabling the "match between runs" option in MaxQuant within a time window of 2 min. For comparison of protein levels between samples, the label-free quantification (LFQ) intensity based method was used (41). For the estimation of protein stoichiometries within a sample, the intensity-based absolute quantification (iBAQ) (25) method was applied. Both values were calculated by the MaxQuant software. All statistical analyses were performed using Microsoft Excel.

#### **Cloning of EPYC1 and RbcS1**

*EPYC1* (Cre10.g436550) and *RBCS1* (Cre02.g120100) ORFs were amplified from gDNA using Phusion Hotstart II polymerase (Thermo Scientific) with the respective EPYC1\_ORF\_F/R or RBCS1\_ORF\_F/R primer pairs (*SI Appendix*, Table S2). Gel purified PCR products, containing vector overlap regions, were cloned into pLM005 or pLM006 by Gibson assembly (42). Final pLM005 constructs are in frame with Venus-3xFLAG and contain the AphVIII gene for paromomycin resistance, final pLM006 constructs are in frame with mCherry-6xHIS and contain the AphVII gene for hygromycin resistance. Both pLM005 and pLM006 confer ampicillin resistance for bacterial selection. For complementation with untagged EPYC1, mCherry-6xHIS was removed from pLM006-EPYC1-mCherry-6xHIS by BglII restriction digestion, gel purified then re-ligated. All constructs were verified by Sanger sequencing. GenBank accession numbers are: pLM005-EPYC1-Venus, KX077944; pLM005-Venus-Cloning-Vector, KX077945; pLM006-EPYC1, KX077946; pLM006-EPYC1-mCherry, KX077947; pLM006-mCherry, KX077948; pLM006-mCherry-Cloning-Vector, KX077949; pLM006-RBCS1-mCherry, KX077950; pMJ016c, KX077951.

#### **Transformation of *Chlamydomonas* for complementation and fluorescence localization of proteins**

Transformation was performed by electroporation as in Zhang *et al.* (37). Nuclear transformation in *Chlamydomonas* occurs by non-homologous insertion of DNA into the genome, resulting in random integration.

For each transformation, 14.5 ng kbp<sup>-1</sup> of EcoRV cut plasmid was mixed with 250 µL of 2 x 10<sup>8</sup> cells mL<sup>-1</sup> at 16 °C and transformed immediately into WT or *epyc1* strains by electroporation. Cells were selected on TAP paromomycin (20 µg mL<sup>-1</sup>) or hygromycin (25 µg mL<sup>-1</sup>) plates and kept in low light (5-10 µmol photons m<sup>-2</sup> s<sup>-1</sup>) until picking or screening for fluorescence lines. In addition, for the complementation of the *epyc1* mutant, a second transformation was selected on TP plates, without antibiotics at low CO<sub>2</sub> (~0.04% v/v CO<sub>2</sub>) under 500 µmol photons m<sup>-2</sup> s<sup>-1</sup> light.

To screen for Venus and mCherry expressing lines, transformations were spread on rectangular plates (Singer Instruments) containing 86 mL of TAP plus antibiotics. Once colonies were ~2-3 mm in diameter, plates were transferred to ~100 µmol photons m<sup>-2</sup> s<sup>-1</sup> light for 24-36 hours and then screened for colony fluorescence on a Typhoon Trio fluorescence scanner (GE Healthcare). Excitation and emission settings were: Venus, 532 excitation with 555/20 emission; mCherry, 532 excitation with 610/30 emission; and chlorophyll autofluorescence, 633 excitation with 670/30 emission. Dual-tag lines were generated sequentially by expressing pLM005-EPYC1-Venus-3xFLAG in WT then adding pLM006-RbcS1-mCherry-6xHIS. To confirm expression of both Venus and mCherry in dual-tag strains and to select for strains with equal fluorescence intensity for the analysis of RbcS1-mCherry localization in WT and *epyc1*, strains were also screened on a Tecan Infinite M1000 PRO (65).

### **Fluorescence microscopy and Rubisco-mCherry mislocalization in the *epyc1* mutant**

All fluorescence microscopy was performed using a spinning disk confocal microscope (3i custom adapted Leica DMI6000) with samples imaged on poly-L-lysine coated plates (Ibidi). The following excitation and emission settings were used: Venus, 514 excitation with 543/22 emission; mCherry, 561 excitation with 590/20 emission; and chlorophyll, 561 excitation with 685/40 emission. Images were analysed using Fiji software. For RbcS1-mCherry localization in WT and the *epyc1* mutant, lines showing equal RbcS1-mCherry fluorescence intensity were chosen for analysis (see above). WT and *epyc1* lines were imaged using the above mCherry and chlorophyll settings. A Z-stack composed of 40 slices 0.3 µm apart was obtained for each field of view. To quantify the percentage of fluorescence signal from outside the pyrenoid region, raw images were analysed as follows: Pixel intensity in the mCherry channel was summed across the 40 Z-sections for cells that were fully sectioned. Using the chlorophyll channel as a reference a cell outline region of interest (ROI; varying between cells) and pyrenoid ROI (set at 2.8 µm in diameter for WT and mutant) were drawn. For each cell, background fluorescence was subtracted by taking the average of 4 measurements surrounding the cell, and autofluorescence was subtracted separately from the pyrenoid and whole cell ROIs by taking the average of 22 WT cells not expressing mCherry. Finally, the percentage RbcS1-mCherry signal from outside of the pyrenoid region was calculated as the  $(total\ cell\ signal - pyrenoid\ signal) / total\ cell\ signal \times 100\%$ .

### **Analysis of gene expression by qRT-PCR**

Total RNA was extracted from 30 µg chlorophyll a+b (~10 mL mid-log cell suspension), using TRIzol Reagent, as per manufacturer's instructions (Life Technologies). Complementary DNA was synthesised from 500 ng of total RNA using SuperScript III Reverse Transcriptase (Life Technologies), RNaseOUT (Life Technologies), and

oligo(dT)18 primers (Thermo Scientific). Relative gene expression was measured in real time in a Rotor-Gene Q thermocycler (Qiagen). Reactions (10  $\mu$ L) used SYBR Green JumpStart Taq ReadyMix (Sigma-Aldrich). Gene expression was calculated according to the method of Livak and Schmittgen (45), relative to the *Chlamydomonas* gene coding for the Receptor of Activated Protein Kinase C1 (RCK1, Cre06.g278222) (46), which is not significantly induced by low-CO<sub>2</sub> (61). All primers used are in *SI Appendix* (Table S2).

### **Screening for the *epyc1* mutant**

The *epyc1* mutant was isolated from a collection of high CO<sub>2</sub> requiring mutants by a pooled screening approach. A collection of approximately 7,500 mutants on 79 plates, each with 96 colonies, was grown in liquid TAP in 96 well plates then pooled by well row, well column, whole plate row and whole plate column to give a total of 38 pools. Pooled cells were pelleted, DNA was extracted by phenol:chloroform:isoamyl alcohol (Phenol:CIA, 25:24:1; Sigma-Aldrich) and then screened by PCR for an EPYC1 mutant using a primer in the pMJ016c mutagenesis cassette (a modified pMJ013c cassette) (37) and a primer in the EPYC1 gene. The identified *epyc1* mutant has an insertion of the pMJ016c resistance cassette in the 5'UTR, the resistance cassette is 11 bp upstream of the ATG start codon, with the cassette having a 10 bp deletion at the 3' end. The upstream gDNA-cassette junction cannot be PCR amplified. However, PCR shows the full cassette is intact and that >397 bp upstream of the insertion site is also intact (Fig S2A). All primers used are in *SI Appendix* (Table S2).

### **Protein extraction and western blotting**

For EPYC1 and CAH3 protein quantification in WT and the *epyc1* mutant, protein was extracted from unfrozen cells, normalised to chlorophyll, separated by SDS-PAGE and western blotted as described in Heinnickel *et al.* (47). Both the primary anti-EPYC1 and anti-CAH3 (Agrisera) antibodies were used at a 1:2,000 concentration and the secondary horseradish-peroxidase (HRP) conjugated goat anti-rabbit (Life Technologies) at a 1:10,000 concentration. To ensure even loading, membranes were stripped (Restore PLUS western blot stripping buffer, Thermo Scientific) and re-probed with anti-tubulin (1:25,000; Sigma) followed by HRP conjugated goat anti-mouse (1:10,000; Life Technologies). The anti-EPYC1 antibody was raised in rabbit to the C-terminal region of EPYC1 (KSKPEIKRTALPADWRKGL-cooh) by Yenzym Antibodies (South San Francisco, California, USA).

For Rubisco quantification in WT and *epyc1* mutant, total soluble proteins were extracted from 300  $\mu$ g chlorophyll (a+b) (~100 mL mid-log cell suspension). Cells were harvested by centrifugation (13,000 g, 10 min, 4°C), re-suspended in ice cold 1.5 mL extraction buffer (50 mM Bicine, pH 8.0, 10 mM NaHCO<sub>3</sub>, 10 mM MgCl<sub>2</sub>, and 1 mM DTT), and lysed by sonication (6 x 30 second bursts of 20 microns amplitude, with 15 s on ice between bursts; Soniprep 150, MSE UK, London, UK). Lysis was checked by inspecting samples under a light microscope. Lysate was clarified by centrifugation (13,000 g, 20 min, 4°C). Protein content was determined using the Bradford method (Sigma Aldrich). Soluble proteins were separated on 12% (w/v) denaturing polyacrylamide gel. Sample loading was normalised by protein amount (10  $\mu$ g per lane), and even loading was controlled by staining a gel with identical protein load (GelCode Blue, Life Technologies). After transfer onto a polyvinylidene difluoride membrane

(Amersham), Rubisco was immuno-detected with a polyclonal primary antibody raised against Rubisco (1:10,000) followed by a HRP conjugated goat anti-rabbit (1:20,000; GE Healthcare).

### **Chlorophyll concentration**

Total pigments were extracted in 100% methanol, and the absorbance of the clarified supernatant (13,000 g, 1 min, 4°C) was measured at 470, 652, 665, 750 nm (UV 300 Unicam, Thermo Spectronic, Cambridge, UK).

Concentration of chlorophyll (a+b) was calculated using the equation of Wellburn (66).

### **Spot tests**

WT, *epyc1* and complemented cell lines were grown in TAP until  $\sim 2 \times 10^6$  cells mL<sup>-1</sup>, washed once with TP, resuspended in TP to a concentration of  $6.6 \times 10^5$  cells mL<sup>-1</sup>, then serially diluted 1:10 three times. 15  $\mu$ L of each dilution was spotted onto four TP plates and incubated in low or high CO<sub>2</sub> with 100 or 500  $\mu$ mol photons m<sup>-2</sup> s<sup>-1</sup> of light for seven days before imaging.

### **Oxygen evolution measurements**

Apparent affinity for inorganic carbon was determined by oxygen evolution (48). Photoautotrophically grown liquid cultures were harvested by centrifugation (2,000 g, 5 min, 4°C) and re-suspended in 25 mM HEPES-KOH (pH 7.3) to a density of  $\sim 1.5 \times 10^8$  cells mL<sup>-1</sup>, as determined by haemocytometer count. Aliquots of cells (1 mL) were added to a Clark-type oxygen electrode chamber (Rank Brothers, Bottisham, UK) attached to a circulating water bath set to 25°C. The chamber was closed for a light pre-treatment (200-300  $\mu$ mol photons m<sup>-2</sup> s<sup>-1</sup> illumination for 10-25 min), to allow cells to deplete any internal inorganic carbon pool. When net oxygen evolution ceased, 10  $\mu$ L of increasingly concentrated NaHCO<sub>3</sub> solution was added to the algal suspension at 30 second intervals, and the rate of oxygen evolution was recorded every second using a PicoLog 1216 data logger (Pico Technologies, St Neots, UK). Cumulative concentrations of sodium bicarbonate after each addition were as follows: 2.5, 5, 10, 25, 50, 100, 250, 500, 1,000, and 2,000 mM. Michaelis-Menten curves were fitted to plots of external inorganic carbon concentration versus the rate of O<sub>2</sub> evolution. The concentration of inorganic carbon required for half maximal rates of photosynthesis (K<sub>0.5</sub>) was calculated from this curve.

### **Pyrenoid area analysis by transmission electron microscopy**

To minimise the loss of biological signal during harvesting, fixative (glutaraldehyde, final 2.5%) was added to cell cultures immediately before harvesting. Cell suspensions containing  $\sim 5 \times 10^7$  cells in mid-log were pelleted (4,000 g, 5 min, 4°C) and fixed in 1 mL tris-minimal medium containing 2.5% glutaraldehyde and 1% H<sub>2</sub>O<sub>2</sub> (30% w/v) for 1 hour on a tube rotator at 4°C. Unless otherwise specified, all following steps were performed at room temperature on a tube rotator. Cells were pelleted (4,000 g 5 min) and washed with ddH<sub>2</sub>O (3X, 5 min). Cells were osmicated for 1 hour in 1 mL 1% (v/v) OsO<sub>4</sub> containing 1.5% (w/v) K<sub>3</sub>[Fe(CN)<sub>6</sub>] and 2 mM CaCl<sub>2</sub>. Cells were pelleted and washed with ddH<sub>2</sub>O (4X, as above). Cells were stained for 1 hour in 1 mL 2% (w/v) uranyl acetate. After pelleting

and washing with ddH<sub>2</sub>O (3X), cells were dehydrated in 70%, 95%, 100% ethanol, and 100% acetonitrile (2X). Cells were embedded in epoxy resin mix, containing Quetol 651, nonenyl succinic anhydride, methyl-5-norbornene-2,3-dicarboxylic anhydride, and dimethyl-benzylamine (all reagents from Agar Scientific, Stansted, UK), in the following proportions: 35%, 46%, 17%, 2%. Resin was refreshed 4 times over two days. Thin sections (50 nm) were prepared by the Cambridge Advanced Imaging Centre (Ms Lyn Carter) on a Leica Ultracut UCT Ultramicrotome and mounted onto 300 mesh copper grids. Samples were imaged with a Tecnai G2 transmission electron microscope (FEI, Hillsboro, OR, USA) at 200 kV. Image analysis (area measurements) was performed using ImageJ. Ten 54  $\mu\text{m}^2$  areas were randomly selected and all pyrenoid positive cells were imaged (WT low CO<sub>2</sub>, 79 out of 271 cells displayed a pyrenoid; *epyc1* low CO<sub>2</sub>, 37 out of 139 cells displayed a pyrenoid; WT high CO<sub>2</sub>, 18 out of 196 cells displayed a pyrenoid; *epyc1* high CO<sub>2</sub>, 22 out of 255 cells displayed a pyrenoid). Cell area was determined by outlining the plasma membrane. Pyrenoid area was taken as the area inside the starch sheath (generally visible in CCM-induced cells) or the electron dense area inside the chloroplast when no starch sheath was visible. Control immuno-gold labelling experiments using a high concentration of primary antibody (1:20) confirmed that these areas had dense concentrations of Rubisco. Pyrenoid area was expressed as a percentage of cell area, and data was obtained in classes of 0.5% increment.

### **Quick-freeze deep-etch EM (QFDEEM)**

#### *Sampling and fixation*

It was ascertained in pilot experiments that pyrenoids fixed by the following procedure are indistinguishable in QFDEEM ultrastructure from unfixed controls. 150 mL of each of air-bubbled cultures and 75 mL of high CO<sub>2</sub>-bubbled cultures were pelleted at 1,000 g for 10 min at RT to produce pellets of ~200  $\mu\text{L}$ . The pellets were resuspended in 6 mL of ice-cold 10 mM HEPES buffer (pH 7) and transferred to a cold 25 mL glass flask. A freshly prepared solution of 4% glutaraldehyde (Sigma-Aldrich G7651) in 10 mM HEPES (pH 7) was added 100  $\mu\text{L}$  at a time, swirling between drops, until 1.5 mL in total had been added. The mixture was then left on ice for 1 hour, with agitation every 10 min. The mixture was pelleted (1000 g, 5 min, 4° C), washed in cold HEPES buffer, pelleted again, and finally resuspended in 6 mL fresh HEPES. Samples were shipped overnight to St. Louis in 15 mL conical screw cap tubes maintained at 0-4° C.

#### *Microscopy*

QFDEEM was performed as in Heuser (44). Briefly, small samples of pelleted cells were placed on a cushioning material and dropped onto a liquid helium-cooled copper block; the frozen material was transferred to liquid nitrogen and then to an evacuated Balzers apparatus, fractured, etched at -80°C for 2 min, and platinum/carbon rotary-replicated. The replicas were examined with a JEOL electron microscope, model JEM 1400, equipped with an AMTV601 digital camera. The images are photographic negatives; hence, protuberant elements of the fractured/etched surface are more heavily coated with platinum and appear whiter.



### **Immunogold-localization of Rubisco**

Resin embedded material previously used for ultra-structural characterization of the pyrenoid was re-cut and thin sections were mounted on nickel grids. Osmium removal and unmasking of epitopes was done by acid treatment (67). Grids were gently floated face down on a droplet (~30  $\mu\text{L}$ ) of 4% sodium meta-periodate (w/v in ddH<sub>2</sub>O) for 15 min, and 1% periodic acid (w/v in ddH<sub>2</sub>O) for 5 min. Each acid treatment was followed by several short washes in ddH<sub>2</sub>O. Non-specific sites were blocked for 5 min in 1% BSA (w/v) dissolved in high-salt tris-buffered saline containing 500 mM NaCl, 0.05% Triton X-100 and 0.05% Tween 20 (hereafter abbreviated HSTBSTT). Salt, detergent, and surfactant concentrations were determined empirically to minimise background signal. Binding to primary antibody was done by incubating grids overnight in 1% BSA in HSTBSTT, with 1:1,000 dilution of the Rubisco antibody. Excess antibody was removed by 15 min washes (2X) in HSTBSTT and 15 min washes (2X) in ddH<sub>2</sub>O. Incubation with secondary antibody (15 nm gold particle-conjugated goat anti-rabbit secondary antibody in 1% BSA in HSTBSTT, 1:250) was done at RT for 1 hr. Excess secondary antibody was removed by washing as above. Thin sections were prepared and imaged as for *Pyrenoid area analysis by transmission electron microscopy*, above. Randomisation was done as above (see TEM) with scoring capped to ~25 cells for each treatment. Non-specific labelling was taken as any particle on a free resin area, i.e. outside a cell. Non-specific density was subtracted from pyrenoid and chloroplast particle density. Fraction of particles in the pyrenoid was calculated as background-adjusted  $n_{\text{pyrenoid}} / (n_{\text{pyrenoid}} + n_{\text{stroma}})$ , where  $n_{\text{stroma}}$  is the number of particles in the stroma to the exclusion of the pyrenoid and the starch sheath. To improve the clarity of gold particles in Fig. 3g, particles were enlarged 10x using the image analysis software, Fiji. Briefly, images were thresholded to isolate individual gold particles, these were then enlarged 10x, and the new image overlaid on the original image with an opacity of 50%.

### **Co-Immunoprecipitations**

WT cells expressing pLM005-Venus-3xFLAG, pLM005-EPYC1-Venus-3xFLAG or pLM005-RbcS1-Venus-3xFLAG were grown in 800 mL of TP plus 2  $\mu\text{g mL}^{-1}$  paromomycin with continual bubbling at low CO<sub>2</sub> (0.04% CO<sub>2</sub>) under 150  $\mu\text{mol photons m}^{-2} \text{ s}^{-1}$  of light until a cell density of ~2-4  $\times 10^6$  cells mL<sup>-1</sup>. Cells were then spun out (2,000 g, 4 min, 4°C), washed in 40 mL of ice cold TP, centrifuged then resuspended in a 1:1 (v/w) ratio of ice-cold 2xIP buffer (400 mM sorbitol, 100 mM HEPES, 100 mM KOAc, 4 mM Mg(OAc)<sub>2</sub>·4H<sub>2</sub>O, 2 mM CaCl<sub>2</sub>, 2 mM NaF, 0.6 mM Na<sub>3</sub>VO<sub>4</sub> and 1 Roche cOmplete EDTA-free protease inhibitor/ 25 mL) to cell pellet. This cell slurry was then added drop wise to liquid nitrogen to form small *Chlamydomonas* “popcorn” balls approximately 5 mm in diameter. These were stored at -70°C until needed.

Cells were lysed by grinding 1g (~500 mg of original cell pellet) of *Chlamydomonas* popcorn balls by mortar and pestle at liquid nitrogen temperatures, for 10 min. The ground cells were defrosted on ice, then dounced 20 times on ice with a Kontes Glass Co. Duall #21 homogenizer. Membranes were solubilized by incrementally adding an equal volume of ice-cold 1xIP buffer plus 2% digitonin (final concentration is 1%), then incubating at 4°C for 40 min with nutation. The lysate was then clarified by spinning for 30 min at full-speed in a table-top centrifuge at 4°C. The supernatant (Input) was then transferred to 225  $\mu\text{L}$  of protein G Dynabeads (Life

Technologies) that had been incubated with anti-FLAG M2 antibody (Sigma) according to the manufacturer's instructions, except 1xIP buffer was used for the wash steps. The Dynabead-cell lysate was incubated for 2.5 hours on a rotating platform at 4°C, then the supernatant removed (Flow-through). The Dynabeads were washed 4 times with 1xIP buffer plus 0.1% digitonin followed by a 30 min elution with 50 µL of 1xIP buffer plus 0.25% digitonin and 2 µg/ µL 3xFLAG peptide (Sigma; 3xFLAG peptide elution) and a 10 min elution in 1x Laemmli buffer with 50 mM beta-mercaptoethanol at 70°C (Boiling elution). Samples were run on 10% SDS-PAGE gels, then silver stained or transferred to PVDF membrane and probed with anti-FLAG (1:2,000; secondary: 1:10,000 HRP goat anti-mouse), anti-Rubisco (1:10,000; secondary: 1:20,000 HRP goat anti-rabbit) or anti-EPYC1 (1:2,000; secondary: 1:10,000 HRP goat anti-rabbit).

### **EPYC1-Rubisco interaction model**

We built a model of the EPYC1-Rubisco interaction using Blender ([www.blender.org](http://www.blender.org)) based on the following logic: If each of the 4 EPYC1 repeats can bind a holoenzyme, the 2 internal repeats would have different linking properties from the 2 terminal repeats. If bound to an internal repeat, a holoenzyme would be directly linked through this EPYC1 protein to 2 other holoenzymes. In contrast, if bound to a terminal repeat, the holoenzyme would only be directly linked through this EPYC1 protein to one other holoenzyme. Therefore on average, each EPYC1 repeat would link one Rubisco holoenzyme to 1.5 other holoenzymes. Given the octameric structure of the Rubisco holoenzyme, a holoenzyme likely has 8 binding sites for EPYC1. Taken together, on average each holoenzyme would be bound to 12 other holoenzymes by 8 EPYC1 proteins, in an arrangement that could expand indefinitely in all directions. A perfect arrangement of this nature would require a stoichiometry of one EPYC1 polypeptide for every four Rubisco small or large subunits.

### **Analysis of other algal proteomes for EPYC1-like physicochemical properties**

Complete translated genomic sequences from pyrenoid and non-pyrenoid algae were downloaded from Uniprot or Phytozome. Protein sequences were then analyzed for tandem repeats using Xstream (53) with default settings except the following were set to: Min Period, 40; Max Period, 80; Min Copy #, 3.0; Min TR Domain, 75; Min Seq Content, 0.7. The pI of the Xstream hits were then batch calculated using the Gene Infinity Protein Isoelectric Point calculator ([http://www.geneinfinity.org/sms/sms\\_proteiniep.html](http://www.geneinfinity.org/sms/sms_proteiniep.html)), the disorder profile calculated using VLXT (54) and the presence of transmembrane domains using TMHMM v. 2.0 (55). Proteins with an oscillating disorder profile with a frequency between 40-80 were classified as potential EPYC1-like Rubisco linker proteins. By applying stringent parameters we have tried to reduce the number of false positive hits but we realize that our approach has several limitations, including: 1) Missing true linker proteins due to not all of the physicochemical properties of EPYC1 being essential for linker function. 2) Incomplete genome assembly of the investigated algae. 3) Incorrect gene models resulting in truncated, mis-spliced and frame-shifted proteins.

### **Statistical methods**

When growing algal material in liquid medium, flasks were placed randomly throughout the orbital shaker/incubator. Placement was randomized after each sub-culturing to offset any differences in illumination quality. Manifold for air/CO<sub>2</sub> delivery had standardized tubing length and internal diameter for even aeration. Cells lysis via sonication required samples to be processed sequentially. Order of processing was randomized.

Sample size of O<sub>2</sub> evolution measurement was aligned to previously published work from the Griffiths Lab (20, 62). Sample size of electron microscopy related experiments (scoring of TEM thin sections and immunogold experiments) was validated by jackknife resampling.

Pre-established exclusion criteria for TEM image scoring were: (i) only grid areas fully covered with material (54 μm<sup>2</sup>) were considered; (ii) sections through broken cells and cell sections with a cross area < 12.5 μm<sup>2</sup> (a circle with 2 μm radius served as a guide) were not scored.

Scoring of electron micrographs: images files were renamed with a random number (RANDBETWEEN function in Microsoft Excel), sorted from high to low, and scored blindly. The original filename appearing on the bottom left of each micrograph was masked during the on-screen processing in ImageJ. Randomly selected images were scored by a second experimenter for independent validation. No systematic bias (over- or underestimation) was measured, and measurements deviated on average only by a couple of percentage points.

Two-tailed Student's *t test* was used to compare affinities for inorganic carbon of WT and *epyc1*, as well as the mislocalization of Rubisco by fluorescence microscopy and EM, because this test is robust to non-normal distributions (68). Welch's *t test* was used to compare pyrenoid sizes, because the WT and mutant groups had substantially different standard deviations (68). Fisher's exact test of independence was used to compare the number of pyrenoids in WT and *epyc*, as this test is appropriate when there are two nominal variables (68).

## SI Appendix References

56. Gorman DS & Levine R (1965) Cytochrome f and plastocyanin: their sequence in the photosynthetic electron transport chain of *Chlamydomonas reinhardtii*. *Proceedings of the National Academy of Sciences of the United States of America* 54(6):1665-1669.
57. Kropat J, *et al.* (2011) A revised mineral nutrient supplement increases biomass and growth rate in *Chlamydomonas reinhardtii*. *The Plant journal : for cell and molecular biology* 66(5):770-780.
58. Spreitzer RJ & Mets L (1981) Photosynthesis-deficient Mutants of *Chlamydomonas reinhardtii* with Associated Light-sensitive Phenotypes. *Plant physiology* 67(3):565-569.
59. Mettler T, *et al.* (2014) Systems Analysis of the Response of Photosynthesis, Metabolism, and Growth to an Increase in Irradiance in the Photosynthetic Model Organism *Chlamydomonas reinhardtii*. *The Plant cell* 26(6):2310-2350.
60. Brueggeman AJ, *et al.* (2012) Activation of the carbon concentrating mechanism by CO<sub>2</sub> deprivation coincides with massive transcriptional restructuring in *Chlamydomonas reinhardtii*. *The Plant cell* 24(5):1860-1875.
61. Fang W, *et al.* (2012) Transcriptome-wide changes in *Chlamydomonas reinhardtii* gene expression regulated by carbon dioxide and the CO<sub>2</sub>-concentrating mechanism regulator CIA5/CCM1. *The Plant cell* 24(5):1876-1893.
62. Mitchell MC, Meyer MT, & Griffiths H (2014) Dynamics of carbon-concentrating mechanism induction and protein relocalization during the dark-to-light transition in synchronized *Chlamydomonas reinhardtii*. *Plant physiology* 166(2):1073-1082.
63. Lowry OH, Rosebrough NJ, Farr AL, & Randall RJ (Protein measurement with the Folin phenol reagent.
64. Laemmli UK (1970) Cleavage of structural proteins during the assembly of the head of bacteriophage T4. *Nature* 227(5259):680-685.
65. Yang W, *et al.* (2014) Alternative acetate production pathways in *Chlamydomonas reinhardtii* during dark anoxia and the dominant role of chloroplasts in fermentative acetate production. *The Plant cell* 26(11):4499-4518.
66. Wellburn AR (1994) The Spectral Determination of Chlorophylls a and b, as well as Total Carotenoids, Using Various Solvents with Spectrophotometers of Different Resolution. *Journal of plant physiology* 144(3):307-313.
67. Skepper J (2000) Immunocytochemical strategies for electron microscopy: choice or compromise. *Journal of microscopy* 199(1):1-36.
68. McDonald JH (2009) *Handbook of biological statistics* (Sparky House Publishing Baltimore, MD).
69. Flombaum P, *et al.* (2013) Present and future global distributions of the marine Cyanobacteria *Prochlorococcus* and *Synechococcus*. *Proceedings of the National Academy of Sciences* 110(24):9824-9829.
70. Not F, *et al.* (2004) A single species, *Micromonas pusilla* (Prasinophyceae), dominates the eukaryotic picoplankton in the Western English Channel. *Applied and Environmental Microbiology* 70(7):4064-4072.
71. Chrétiennot-Dinet M, *et al.* (1995) A new marine picoeucaryote: *Ostreococcus tauri* gen. et sp. nov.(Chlorophyta, Prasinophyceae). *Phycologia* 34(4):285-292.

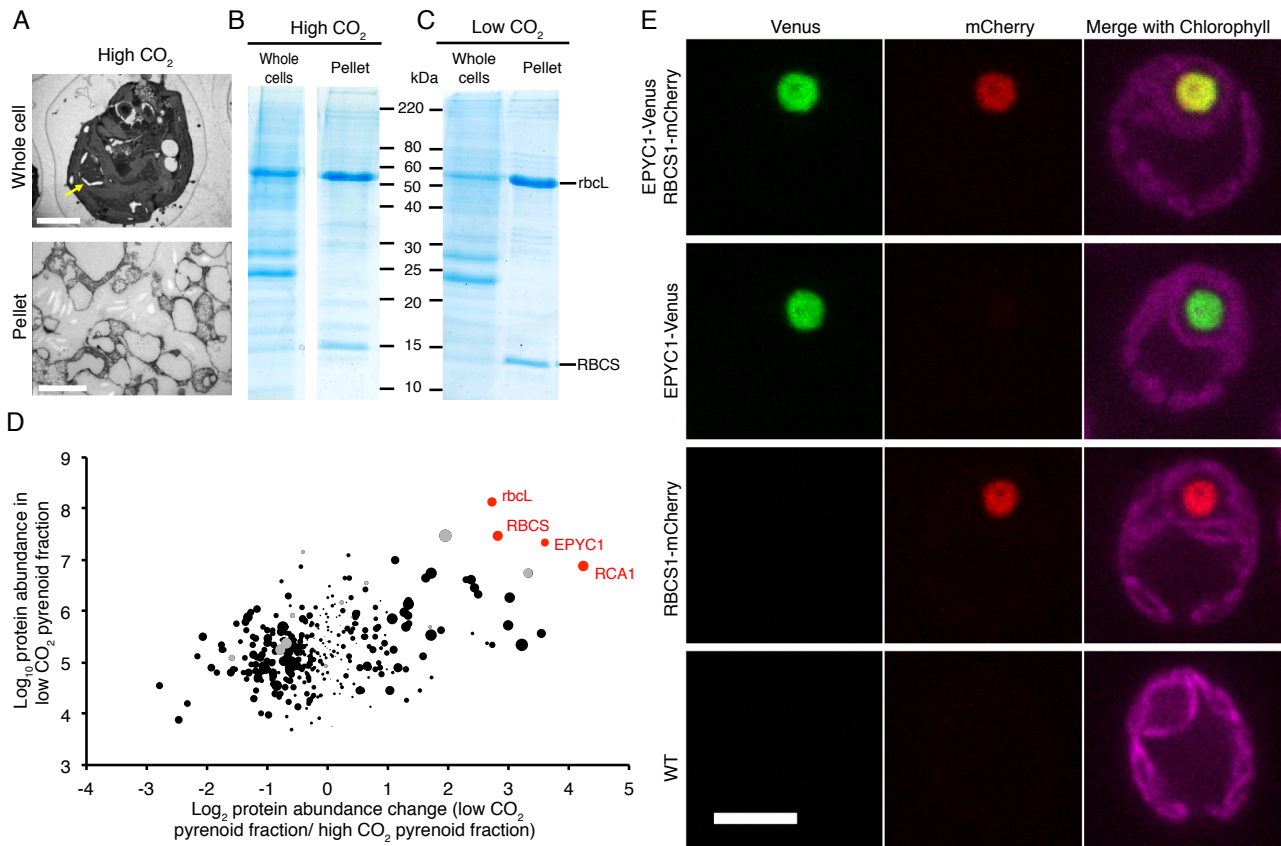


**Fig. S1.** EPYC1 is an abundant pyrenoid component. (A) TEM images of *Chlamydomonas reinhardtii* whole cells and pyrenoid-enriched pellet from cells grown at high CO<sub>2</sub>. Yellow arrow indicates pyrenoid. (Scale bars: 2 μm.) (B) Coomassie-stained SDS-PAGE of whole cell and pyrenoid-enriched pellet at high CO<sub>2</sub>. (C) Coomassie-stained SDS-PAGE of whole cell and pyrenoid-enriched pellet at low CO<sub>2</sub>. (D) Additional analysis of the mass spectrometry data shown in Fig. 1B and Dataset S1. The x-axis is the label-free quantification (LFQ) enrichment in the low-CO<sub>2</sub> pellet fraction relative to the high CO<sub>2</sub> pellet fraction. The iBAQ given on the y-axis, represents the absolute protein abundance in the low-CO<sub>2</sub> pellet. Red data points highlight RbcL, RBCS, EPYC1 and RCA1. Grey circles depict sets of peptides represented by more than one protein due to high sequence similarities, whereas black circles are peptides representing a single protein. Dot sizes indicate the log<sub>10</sub> *P*-value between low CO<sub>2</sub> and high CO<sub>2</sub> pellet fractions (Student's *t* test). In total 366 proteins were identified in all four replicates of both the low- and high-CO<sub>2</sub>-grown pellets. (E) Confocal microscopy of EPYC1-Venus and RBCS1-mCherry co-expressed and individually expressed in WT cells. All images were taken and processed with the same settings. Top panel is the same cell as shown in Fig. 1C. (Scale bar: 5 μm.)

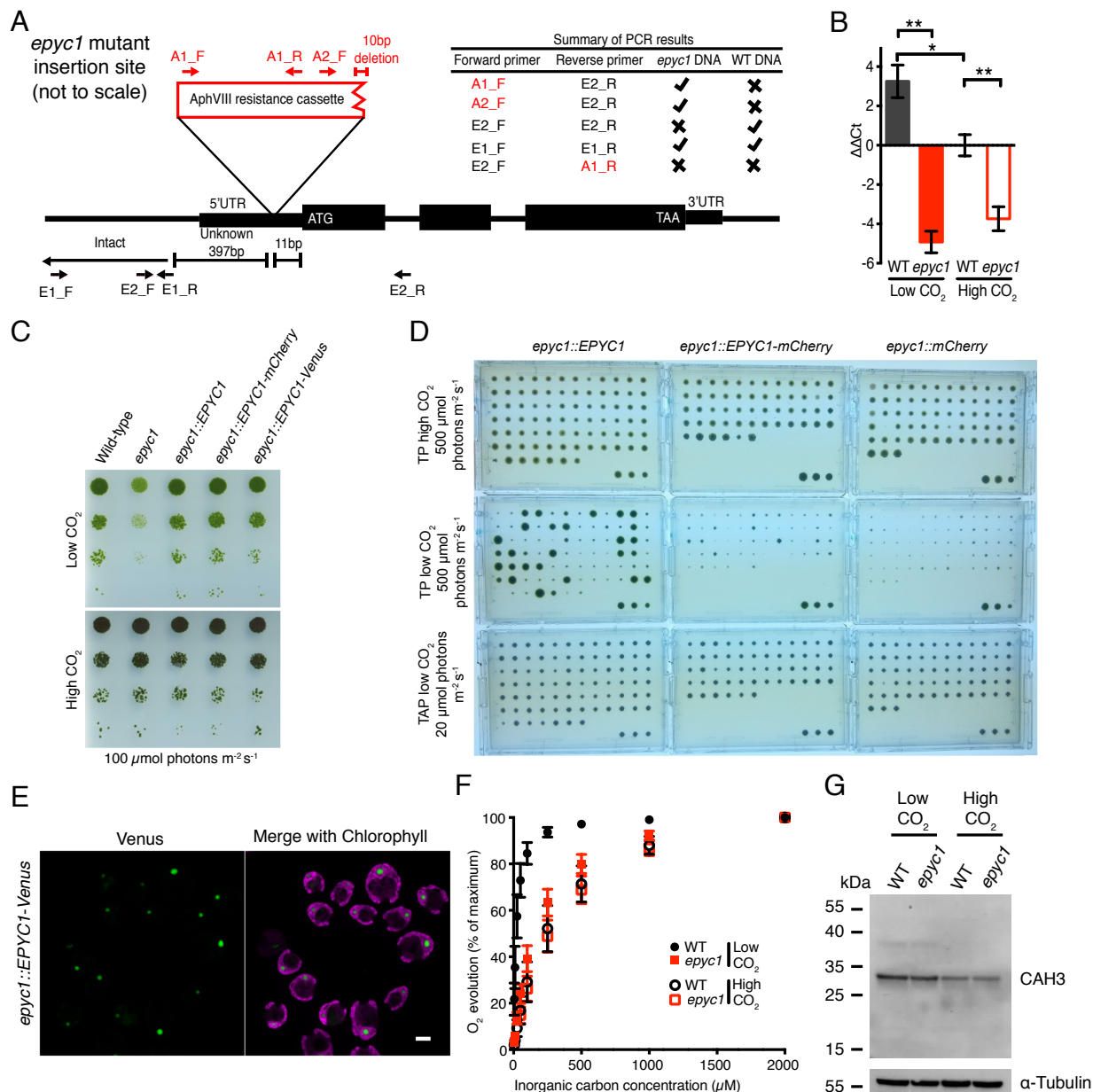


**Fig. S2.** Characterization and complementation of the *epyc1* mutant. (A) Cartoon of the *epyc1* mutant insertion site. The pMJ016c resistance cassette conferring paromomycin through the AphVIII gene is 11 bp upstream of the *EPYC1* ATG start codon. The resistance cassette has a known 10 bp deletion at the 3' end and is fully intact. The junction of the 3' cassette end and the *EPYC1* gene can be amplified with a forward primer annealing at the 5' end of the cassette (A1\_F) and a reverse primer in the *EPYC1* gene (E2\_R). The 5' end of the insert is still uncharacterized. Primers upstream of the insertion site fail to give PCR products when paired with reverse primers in the resistance cassette (e.g. E2\_F and A1\_R). It is known that insertion sites can undergo large insertions and/or deletions in *Chlamydomonas* (37). However, a large deletion upstream of the insertion site is ruled out due to the amplification of a region upstream of the insertion site (E1\_F and E1\_R) in the *epyc1* mutant. Note the cartoon is not to scale for clarity. (B) Quantification of *EPYC1* transcript levels in WT and the *epyc1* mutant at low and high CO<sub>2</sub> by qRT-PCR. Transcript levels are normalized to the reference gene *RCK1*, and plotted relative to WT at high CO<sub>2</sub>. In the *epyc1* mutant, transcript levels were ~250-fold lower than in WT at low CO<sub>2</sub>; and transcript levels were not significantly upregulated between low and high CO<sub>2</sub> ( $P = 0.129$ , Student's *t* test). Data is the mean of 3 biological replicates each measured in triplicate. Error bars: SEM \* indicates  $P < 0.05$ , \*\* indicates  $P < 0.005$ , Student's *t* test. (C) Growth phenotypes of WT, *epyc1* and 3 *epyc1* complemented lines at 100 μmol photons m<sup>-2</sup> s<sup>-1</sup> light intensity. Serial 1:10 dilutions of WT, *epyc1*, *epyc1::EPYC1*, *epyc1::EPYC1-mCherry* and *epyc1::EPYC1-Venus* lines were spotted on TP minimal plates and grown at low and high CO<sub>2</sub> under 100 μmol photons m<sup>-2</sup> s<sup>-1</sup>. (D) Complementation screening of the *epyc1* mutant. The *epyc1* mutant was transformed with pLM006-EPYC1,

pLM006-EPYC1-mCherry or pLM006-mCherry and selected on TAP plates with hygromycin. Hygromycin resistant colonies were picked into a 96 format and propagated twice on TAP with hygromycin plates to allow even growth of all colonies. Colonies were then replicated onto TP or TAP plates and incubated as shown for 12 days before imaging. pLM006-EPYC1 fully rescued the *epyc1* mutant in 28% (22/79) of cases and partially rescued the mutant in 10% (8/79) of cases. pLM006-EPYC1-mCherry partially rescued the mutant in 20% (11/54) of cases. The negative control, pLM006-mCherry, failed to rescue the mutant (0/62). Partially rescued colonies were colonies that were visibly smaller in size than WT but larger in size than negative control colonies. The residual growth seen in all colonies at low CO<sub>2</sub> is carryover from the initial pinning from TAP plates. The 3 bottom right colonies are WT controls. (E) Confocal microscopy of the *epyc1::EPYC1-Venus* complemented line used for spot tests in Fig. 2B. Cells were grown mixotrophically in TAP media and imaged by confocal microscopy as in the materials and methods section. (Scale bar: 5 μm.) (F) The *epyc1* mutant has reduced inorganic carbon affinity. WT and *epyc1* cells were grown photoautotrophically at low and high CO<sub>2</sub>, and whole cell inorganic carbon affinity was measured by O<sub>2</sub> evolution with step-wise increases in inorganic carbon. The K<sub>0.5</sub> values shown in Fig. 2C are derived from these curves. Data is a mean of 5 low CO<sub>2</sub> or 3 high CO<sub>2</sub> biological replicates. For clarity the data has been plotted as a percentage of maximum with the raw data provided in *SI Appendix* (Table S4). Error bars: SD. (G) CAH3 protein levels in WT and *epyc1* mutant cells grown at low and high CO<sub>2</sub> were probed by western blotting with anti-CAH3 antibodies. Anti-tubulin is shown as a loading control.

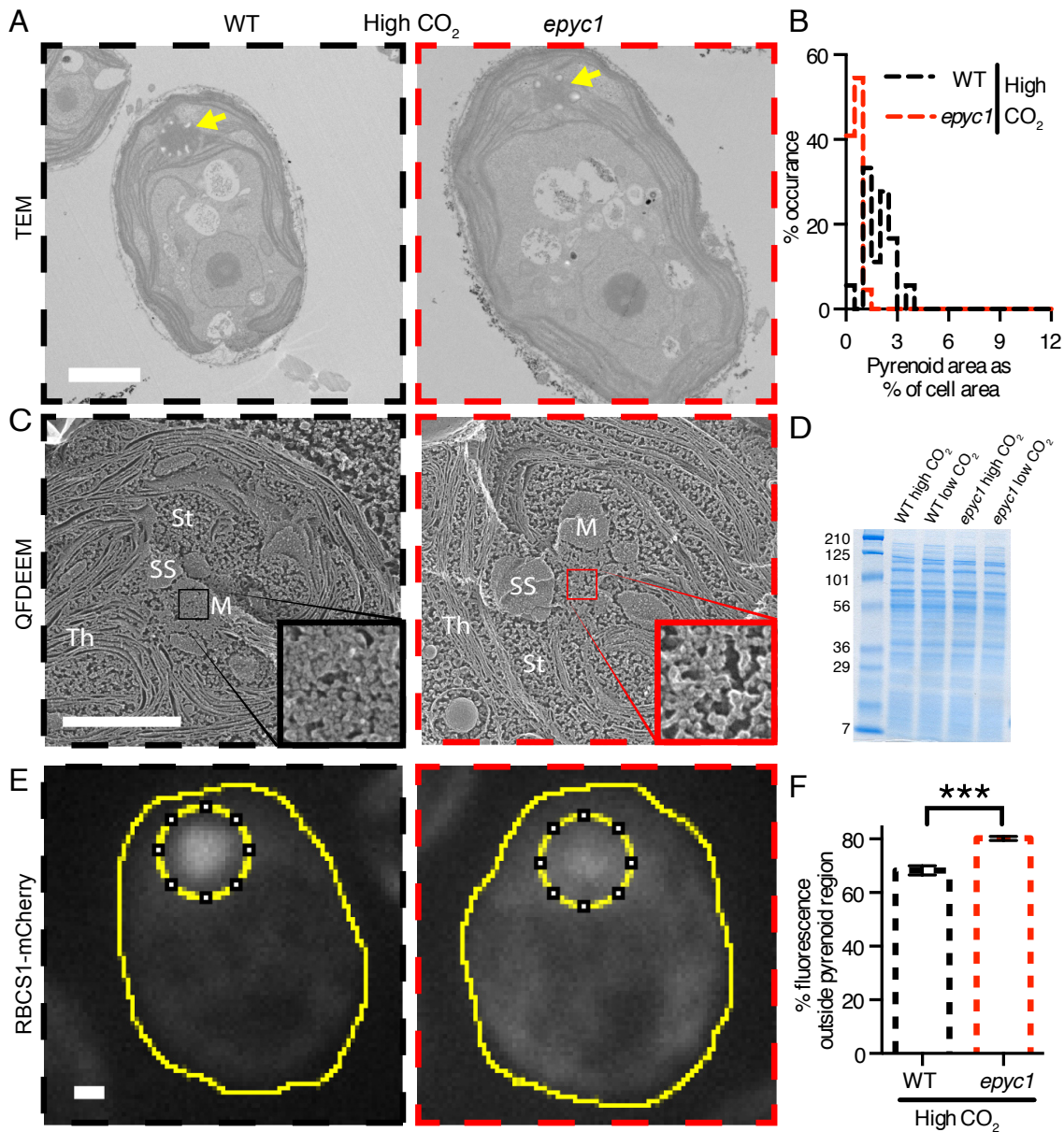


**Fig. S3.** Rubisco is mislocalized in the *epyc1* mutant at high CO<sub>2</sub>. (A) Representative TEMs of WT and *epyc1* cells grown at high CO<sub>2</sub>. Yellow arrows indicate pyrenoids. (B) Quantification of pyrenoid area as percentage of cell area of WT and *epyc1* cells grown at high CO<sub>2</sub> (WT:  $n = 18$ , *epyc1*:  $n = 22$ ,  $P < 10^{-5}$ , Welch's *t* test). (C) Quick-Freeze Deep-Etch EM (QFDEEM) of the pyrenoid of WT and *epyc1* cells grown at high CO<sub>2</sub>. M, pyrenoid matrix; St, stroma; Th, thylakoids; SS, starch sheath. Insets are a 400% zoom of the pyrenoid matrix. (D) Coomassie stained SDS-PAGE loading control gel for samples used in Fig. 3D. (E) The localization of Rubisco was determined by microscopy of WT and *epyc1* mutants containing RBCS1-mCherry at high CO<sub>2</sub>. (F) The fraction of RBCS1-mCherry signal from outside the pyrenoid region (inner dotted line, E) was quantified in WT and *epyc1*. The sum of fluorescence signal from Z stacks is shown and was used for quantitation. WT:  $n = 20$ , *epyc1*:  $n = 20$ , \*\*\* represents  $P = 10^{-6}$ , Student's *t* test. (Scale bars: 1  $\mu\text{m}$ .)



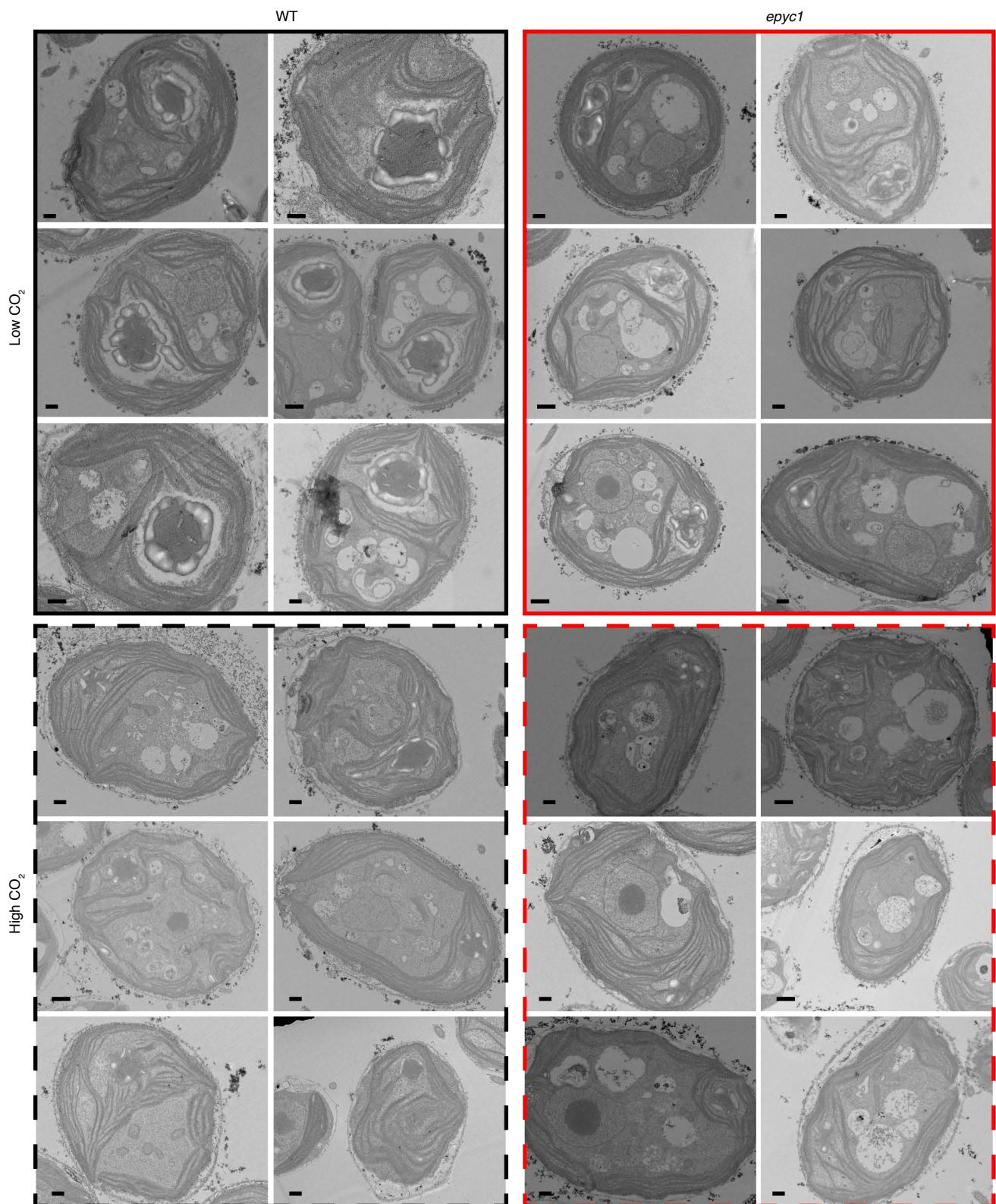


**Fig. S4.** Representative TEM images of WT and *epyc1* cells at low and high CO<sub>2</sub>. A representative selection of TEM images used for pyrenoid area analysis. Cells were prepared and imaged for TEM as in the materials and methods. (Scale bars: 500 nm.)

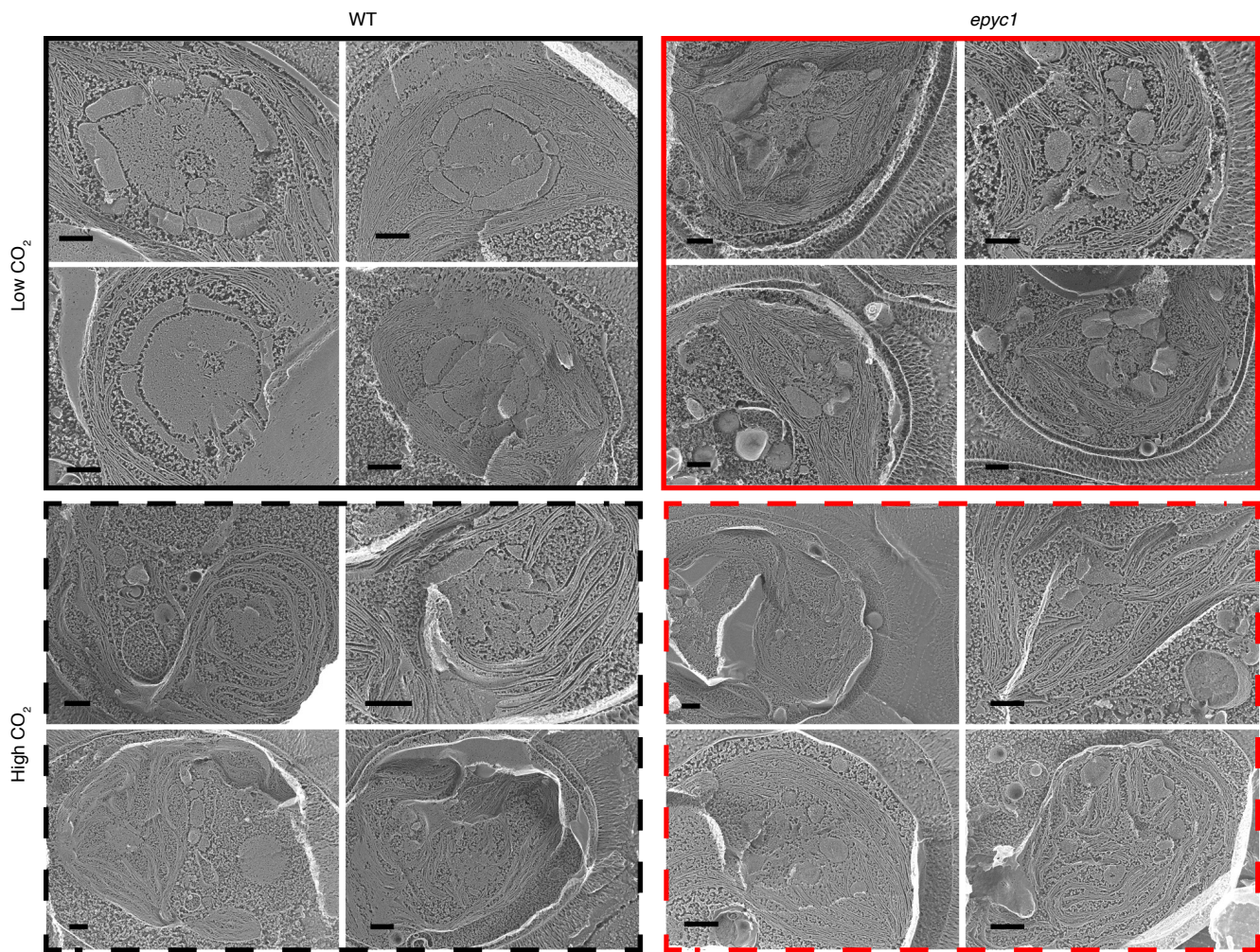


**Fig. S5.** Representative Quick-Freeze Deep-Etch EM (QFDEEM) images of WT and *epyc1* cells at low and high CO<sub>2</sub>. Cells were prepared and imaged for QFDEEM as described in the materials and methods. (Scale bars: 500 nm.)

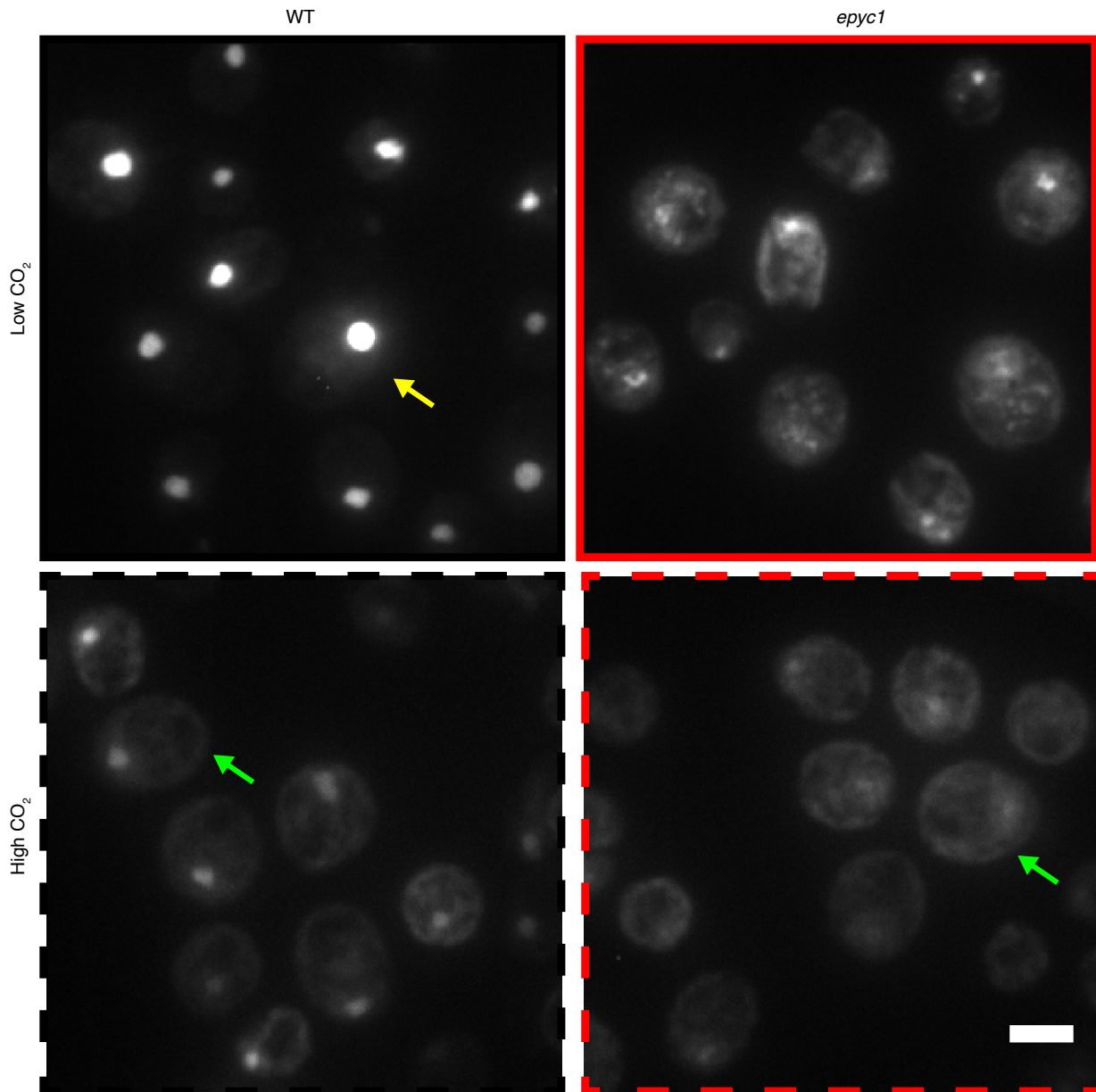


**Fig. S6.** Representative cells used for Rubisco-mCherry localization data. A representative field of view used for quantifying the mislocalization of Rubisco in the *epyc1* mutant. Images are summed z-stacks of 40 confocal sections 0.3  $\mu\text{m}$  apart. Yellow arrow indicates the cell used for Fig. 3E. Green arrows indicate cells used for Fig. S3E. (Scale bar: 5  $\mu\text{m}$ .)

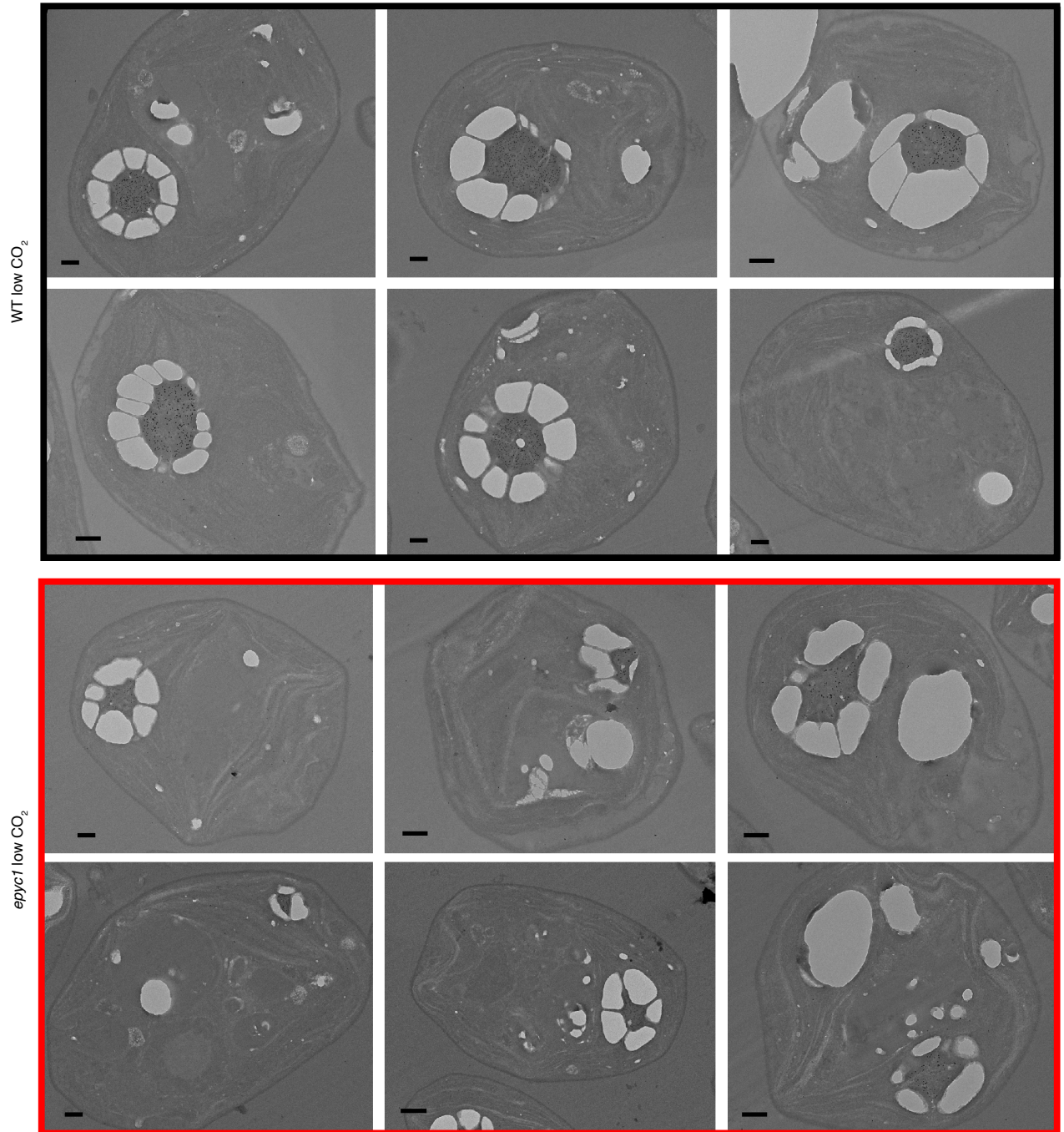


**Fig. S7.** Representative cells used for Rubisco immunogold labeling. A representative selection of immunogold-TEM images used for quantification of Rubisco levels outside the pyrenoid. The top left cell for each condition is the cell used in Fig. 3G before gold particle enlargement. Cells were prepared and imaged for immunogold-TEM as outlined in the materials and methods. (Scale bars: 500 nm.)

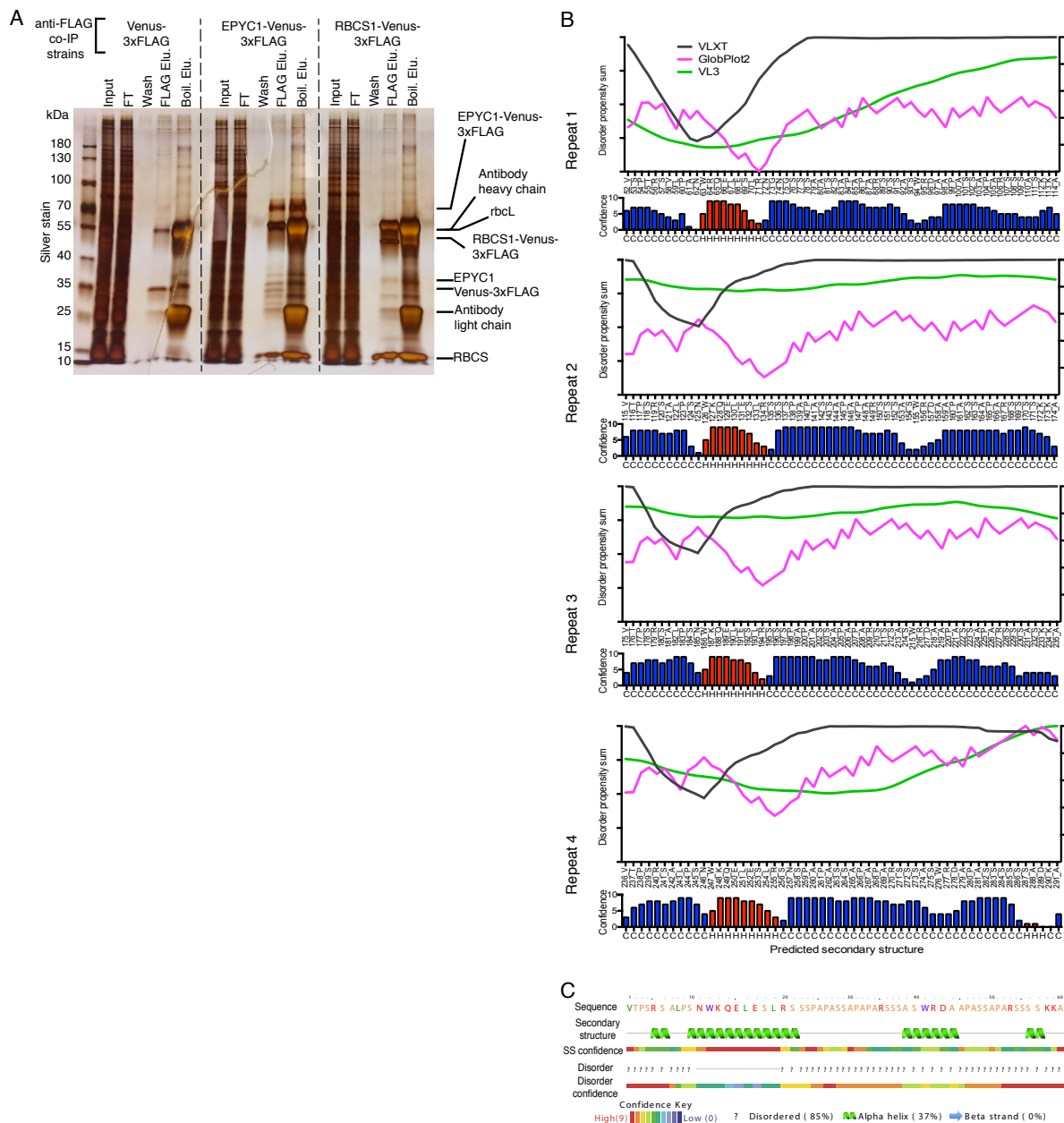


**Fig. S8.** EPYC1 interactions and sequence analysis. (A) Anti-FLAG co-immunoprecipitations (co-IPs) of WT cells expressing Venus-3xFLAG, EPYC1-Venus-3xFLAG and RBCS1-Venus-3xFLAG are shown. For each co-IP, the input, flow-through (FT), 4<sup>th</sup> wash (wash), 3xFLAG elution (FLAG Elu.) and boiling elution (Boil. Elu.) were run on an SDS-PAGE gel and silver stained. Right hand side labels show the expected sizes of proteins. (B) and (C) Analysis of the EPYC1 protein sequence. (B) To investigate the disorder of EPYC1, the full-length amino acid sequence was analyzed by VL3, VLTX and GlobPlot2 disorder prediction algorithms. The lower bar chart shows the PSIPRED v3.3 predicted secondary structure of full-length EPYC1, H = helix (red), C = coil (blue). Bar height indicates confidence value. (C) Analysis of the repeat region from 115-174 by Phyre2.

**Table S1. The contribution of the pyrenoid to global net primary production (NPP)**

	Percentage of ocean NPP	Percentage of algal group with a pyrenoid	Percentage of ocean NPP mediated by a pyrenoid	Percentage of total NPP
Global primary production				100%
Terrestrial				50 (13) - 54% (3)
Ocean				46 (3) - 50% (13)
Cyanobacteria (Prokaryotic)	10 (14) - 25% (69)			
Eukaryotic algae	75 (69) - 90% (14)			
Diatoms	42 (14, 69) - 50% (14)	100% (15)	42-50%	
Coccolithophores	17 (14, 69) -20% (14)	100% (16)	17-20%	
Chlorophytes	17 (14, 69) -20% (14)	10-90%*	2-18%	
Pyrenoid containing algae			61-88%	28 – 44%

\*The majority of chlorophytes are known to have pyrenoids (17), with the pyrenoid containing *Micromonas pusilla* shown to be the dominant species in several oceanic and coastal regions (70). However, some ocean chlorophytes, including the abundant species *Bathycoccus prasinos*, appear to lack pyrenoids (17).

**Table S2. Oligonucleotides used in this work**

<b>Primer name</b>	<b>Sequence</b>
EPYC1_ORF_F	GCTACTCACAACAAGCCCAGTTATGGCCACTATCTCGTCGATGCGC
EPYC1_ORF_R	GAGCCACCCAGATCTCCGTTACAGGCCCTTGCGCCAGTCAGC
RBCS1_ORF_F	GCTACTCACAACAAGCCCAGTTATGGCCGCCGTCATTGCCAAGTC
RBCS1_ORF_R	GAGCCACCCAGATCTCCGTTACAGGAGCGCTTGTTGGCGGG
GBLP_F:	AACACCGTGACCGTCTCC
GBLP_R:	TGCTGGTGATGTTGAACTCG
EPYC1_F:	AAGCAGCTTGCCTAACCAGCAG
EPYC1_R:	ACATAACACACGCGTACCAAGGC
A1_F	GTTGGATGCACTAGTCACACGAGC
A2_F (EPYC1_Screen_pMJ016c_F)	GACGTTACAGCACACCCTTG
A1_R	GCACCAATCATGTCAAGCCT
E1_F	TCCTCCGCACCAAACATG
E2_F	CATAAGCTGTGAGCCGTTGA
E1_R	CAACTCAGTCAACGGCTCAC
E2_R (EPYC1_Screen_Gene_R)	ACAGTCGCATCAGAAAGGCT

**Table S3. Raw qRT-PCR data**

Gene	cDNA	Replica 1		Replica 2		Replica 3	
		Ct	Mean	Ct	Mean	Ct	Mean
Reference <i>RCK1/Cblp</i> (Cre06.g278222)	WT High CO <sub>2</sub>	12.82	13.14	14.83	15.04	16.36	15.89
		13.3		15.35		15.6	
		13.31		14.93		15.7	
	<i>epyc1</i> High CO <sub>2</sub>	12.77	12.80	15.67	15.52	15.42	15.46
		12.82		15.41		15.38	
		12.81		15.48		15.58	
	WT Low CO <sub>2</sub>	11.44	11.03	13.79	14.06	13.76	14.03
		11		14.48		14.53	
		10.65		13.92		13.81	
	<i>epyc1</i> Low CO <sub>2</sub>	11.28	11.54	14.55	14.67		14.66
		11.53		14.63		14.67	
		11.82		14.84		14.65	
<i>EPYC1</i>	WT High CO <sub>2</sub>	18.28	18.52	19.56	19.63	21.87	21.80
		18.5		19.64		21.8	
		18.78		19.68		21.73	
	<i>epyc1</i> High CO <sub>2</sub>	22.19	22.43	23.74	23.62	24.64	24.81
		21.98		23.66		25.14	
		23.13		23.46		24.66	
	WT Low CO <sub>2</sub>	13.42	13.30	14.74	14.75	17.08	17.22
		13.25		14.75		17.52	
		13.24		14.75		17.06	
	<i>epyc1</i> Low CO <sub>2</sub>	22.64	22.47	24.28	24.22	24.87	24.82
		22.34		23.96		24.62	
		22.44		24.43		24.98	



**Table S4. Raw O<sub>2</sub> evolution data**

		Rate of O <sub>2</sub> evolution (μmol.mg Chl <sup>-1</sup> .h <sup>-1</sup> )										% of maximum													
		WT					epyc					WT					epyc								
	μM*Ci	R1	R2	R3	R4	R5	R1	R2	R3	R4	R5	R1	R2	R3	R4	R5	mean	stdev	R1	R2	R3	R4	R5	mean	stdev
Low CO <sub>2</sub>	2.5			5			3	17	11		2			3			3		2	11	9		2	6	5
	5	27	16	7	2	30	16		9	39	5	14	9	5	1	14	8	5	11		8		5	8	3
	10	63	53	57	70	39	24	22	6		9	32	29	39	45	18	33	10	17	15	5		10	12	5
	25	77	76	77	92	92	34		24	15	21	40	42	53	59	42	47	8	23		20	15	24	21	4
	50	150	117		138	119	25		32	13	18	77	65		89	54	71	15	17		27	13	21	20	6
	100	159	127	142	132	131	69	73	65	49	41	82	71	97	85	60	79	14	47	49	55	49	48	50	3
	250		170	147	133	129	74	79	80	68	66		95	100	86	59	85	18	50	54	68	68	76	63	11
	500	149		131	145	192	78	93	90	90	72	77		89	93	87	87	7	53	63	76	90	83	73	15
	1000	194	151	137	156	220	148	147	118	89	87	100	84	94	100	100	96	7	100	100	100	89	100	98	5
2000		180	141	148	189		129		100	67		100	96	95	86	94	6		87		100	78	88	11	
High CO <sub>2</sub>	50	8	4	2			3	12	8			12	7	4			8	4	3	14	8			8	5
	100	31	7	8			38	23	15			44	12	13			23	18	36	26	17			26	10
	250	50	30	28			68	39	33			71	51	47			56	13	64	45	37			49	14
	500	57	45	52			80	67	69			79	76	88			81	6	76	76	77			76	0
	1000	71	55	60			100	74	82			100	94	100			98	4	95	84	91			90	6
	2000	69	58	55			106	88	90			97	100	92			96	4	100	100	100			100	0

\*Ci: Inorganic carbon

**Table S5. Quantification of number of cells with multiple pyrenoids**

WT Low CO <sub>2</sub>				<i>epyc1</i> Low CO <sub>2</sub>			
Image name	Total cells scored	Cells with >1 pyrenoid	Cells with 1 pyrenoid	Image name	Total cells scored	Cells with >1 pyrenoid	Cells with 1 pyrenoid
2015Feb23Freq25	30	1	12	2015Feb23Freq25	26	0	13
2015Feb23Freq24	24	0	11	2015Feb23Freq24	22	1	8
2015Feb23Freq23	26	0	7	2015Feb23Freq23	21	0	5
2015Feb23Freq22	30	0	13	2015Feb23Freq22	28	1	8
2015Feb23Freq21	17	0	8	2015Feb23Freq21	21	0	10
2015Feb23Freq20	22	0	5	2015Feb23Freq20	26	1	8
2015Feb23Freq19	25	0	9	2015Feb23Freq19	31	3	14
2015Feb23Freq18	26	2	10	2015Feb23Freq18	29	2	12
2015Feb23Freq17	25	1	7	2015Feb23Freq17	23	1	12
2015Feb23Freq16	28	0	12	2015Feb23Freq16	26	0	9
2015Feb23Freq15	23	0	11	2015Feb23Freq15	21	0	6
2015Feb23Freq14	20	0	10	2015Feb23Freq14	25	0	4
2015Feb23Freq13	27	0	15	2015Feb23Freq13	20	0	6
2015Feb23Freq12	23	0	8	2015Feb23Freq12	25	2	8
2015Feb23Freq11	22	1	12	2015Feb23Freq11	23	2	10
2015Feb23Freq10	24	0	10	2015Feb23Freq10	22	0	9
2015Feb23Freq9	22	0	9	2015Feb23Freq9	30	4	15
2015Feb23Freq8	26	0	10	2015Feb23Freq8	25	0	7
2015Feb23Freq7	24	0	6	2015Feb23Freq7	24	1	8
2015Feb23Freq6	30	0	17	2015Feb23Freq6	29	1	11
2015Feb23Freq5	22	0	7	2015Feb23Freq5	34	1	10
2015Feb23Freq4	21	1	6	2015Feb23Freq4	30	3	11
2015Feb23Freq3	24	0	12	2015Feb23Freq3	26	1	9
2015Feb23Freq2	37	1	12	2015Feb23Freq2	29	3	8
2015Feb23Freq1	25	1	13	2015Feb23Freq1	18	2	10
TOTAL	623	8	252	TOTAL	634	29	231
% of cells with multiple pyrenoids			3.2%	% of cells with multiple pyrenoids			12.6%

**Table S6. Analysis of pyrenoid positive and pyrenoid negative algae for proteins with EPYC1-like physicochemical properties**

Species (Phylum)	Pyrenoid	Number of proteins with...				Uniprot or phytozome protein ID	Protein characteristics				Consensus repeat sequence from Xstream	Disorder profile*
		...>=3 repeats with a 40-80aa repeat length...	...and a pI >8...	...and an oscillating disorder profile...	...and no transmembrane domains		Length	Repeat length	Repeat copy #	pI		
<i>Chlamydomonas reinhardtii</i> (Chlorophyta)	Y	18	8	1	1	Cre10.g436550 (EPYC1)	318	61	3.84	11.8	VTPSRALPSN WKQELSLRSS SPAPASSAPAP ARSSASWRDA APASSAPARSS SASKKA	
<i>Thalassiosira pseudonana</i> (Heterokontophyta)	Y	4	1	1	1	B8CF53_THAPS	376	53	6.21	9.1	LSSKPSSAPFVR SEKPSAPSDS PSASVAPTLETS FSPSSSGQPSP MTSESPS	
<i>Phaeodactylum tricornutum</i> (Heterokontophyta)	Y	12	1	1	1	B7GDW7_PHATC	380	46	7.17	9.9	TGPSMTGPSDS DDRRRLRSPST GPSLTGPSMTG PSATGPSMTG SM	
<i>Emiliania huxleyi</i> (Haptophyta)	Y	99	10	2	2	R1G412_EMIHU	353	70	4.10	12.1	PYLPISPARLAR GSTSPHLSPLP ISPHISRTARSR FHIAPSLPISPHI SPTAPHGFHEA PHLPISPHLS	
						R1D601_EMIHU	255	60	3.70	10.1	WTAADDALVKA GQEAGESWVDI AKRLPGRSADS VKRSRNRLKRQ PDTSVKHEPVK RELVR	
<i>Ostreococcus tauri</i> (Chlorophyta)	Y/N†	3	3	2	2	A0A096PAN3_OSTTA	407	63	5.02	11.1	MAASKLGSKNA STRPTVGSTLD ASALTPPSLRFT TENNIHSVPTAF GVADRPASRRV LRREDA	
						A0A090M8K8_OSTTA	470	63	6.02	11.2	MAASKLGSKNA STRPTVGSTLD ASALTPPSLRFT TENNIHSVPTAF GVADRPASRRV LRREDA	
<i>Micromonas pusilla</i> (Chlorophyta)	Y	6	0	0	0							
<i>Chlorella variabilis</i> (Chlorophyta)	Y	3	2	1	0							
<i>Chlorella protothecoides</i> (Chlorophyta)	N	1	0	0	0							
<i>Cyanidioschyzon merolae</i> (Rhodophyta)	N	0	0	0	0							
<i>Galdieria sulphuraria</i> (Rhodophyta)	N	2	0	0	0							
<i>Nannochloropsis gaditana</i> (Heterokontophyta)	N	3	0	0	0							

\*Disordered profiles are a plot of disorder propensity (y axis; 0-1; 0 = ordered, 1 = disordered) against amino acid number (x-axis; 0-437). All profiles are on the same scale. †TEM images of *Ostreococcus tauri* show a singular starch deposit typical of a pyrenoid, however a Rubisco matrix has yet to be confirmed (71).